Adele D'Amico ORCID iD: 0000-0003-2438-2624

Daria Diodato ORCID iD: 0000-0003-3607-8523

Rosalba Carrozzo ORCID iD: 0000-0002-3327-4054

Clinical-genetic features and peculiar muscle histopathology in infantile *DNM1L*-related mitochondrial epileptic encephalopathy

Daniela Verrigni[1]*, Michela Di Nottia[1]*, Anna Ardissone[2,3*], Enrico Baruffini[4*], Alessia Nasca[5], Andrea Legati[5], Emanuele Bellacchio[6], Gigliola Fagiolari[7], Diego Martinelli[8], Lucia Fusco[9], Domenica Battaglia[10], Giulia Trani[1], Gianmarco Versienti[5], Silvia Marchet[5], Alessandra Torraco[1], Teresa Rizza[1], Margherita Verardo[1], Adele D'Amico[1], Daria Diodato[1], Isabella Moroni[2], Costanza Lamperti[5], Stefania Petrini[11], Maurizio Moggio[7], Paola Goffrini[4], Daniele Ghezzi[5,12#], Rosalba Carrozzo[1#], Enrico Bertini[1#]

[1]Unit of Muscular and Neurodegenerative Disorders, Laboratory of Molecular Medicine, Bambino Gesù Children's Hospital, IRCCS, Rome, Italy;

[2]Child Neurology Unit, Fondazione IRCCS Istituto Neurologico Carlo Besta, Milan, Italy;

[3]Department of Molecular and Translational Medicine DIMET, University of Milan-Bicocca, Milan, Italy;

[4]Department of Chemistry, Life Sciences and Environmental Sustainability, University of Parma, Parma, Italy;

[5]Unit of Medical Genetics and Neurogenetics, Fondazione IRCCS Istituto Neurologico Carlo Besta, Milan, Italy

This article has been accepted for publication and undergone full peer review but has not been through the copyediting, typesetting, pagination and proofreading process, which may lead to differences between this version and the Version of Record. Please cite this article as doi: 10.1002/humu.23729.

[6]Genetics and Rare Diseases, Research Division, Bambino Gesù Children's Hospital, IRCCS, Rome, Italy

[7]Unit of Neuromuscular and Rare Disorders, Fondazione IRCCS Ca' Granda Ospedale Maggiore Policlinico, Università of Milano

[8]Division of Metabolism, Bambino Gesù Children's Hospital, IRCCS, Rome, Italy;

[9]Neurophysiology Unit, Department of Neuroscience, Bambino Gesu' Children's Hospital, Rome, Italy

[10]Child Neurology and Psychiatry, Catholic University, Rome, Italy

[11]Research Laboratories, Bambino Gesù Children's Hospital, IRCCS, Rome, Italy.

[12]Department of Pathophysiology and Transplantation, University of Milan, Milan, Italy

* contributed equally to this work.

# These authors contributed equally as senior authors

Correspondence: Enrico Bertini, Unit of Muscular and Neurodegenerative Disorders, Laboratory of Molecular Medicine, Bambino Gesù Children's Hospital, IRCCS, Viale di San Paolo 15, 00146 Rome, Italy, ph +39-06-68593599; Fax: +39-06-68592024; e-mail: bertini@opbg.net

ABSTRACT

Mitochondria are highly dynamic organelles, undergoing continuous fission and fusion. The *DNM1L* gene encodes for the DRP1 protein, an evolutionary conserved member of the dynamin family, responsible for fission of mitochondria, and having a role in the division of peroxisomes, as well. DRP1 impairment is implicated in several neurological disorders and associated with either *de novo* dominant or compound heterozygous mutations. In five patients presenting with severe epileptic encephalopathy we identified 5 *de novo* dominant *DNM1L* variants, the pathogenicity of which was validated in a yeast model. Fluorescence microscopy revealed abnormally elongated mitochondria and aberrant peroxisomes in mutant fibroblasts, indicating impaired fission of these organelles. Moreover, a very peculiar finding in our cohort of patients was the presence,

in muscle biopsy, of core like areas with oxidative enzyme alterations, suggesting an abnormal distribution of mitochondria in the muscle tissue.

Graphical Abstract

DNM1L de novo dominant variants impaired mitochondrial fission and produced abnormal distribution of mitochondria in the muscle tissue.

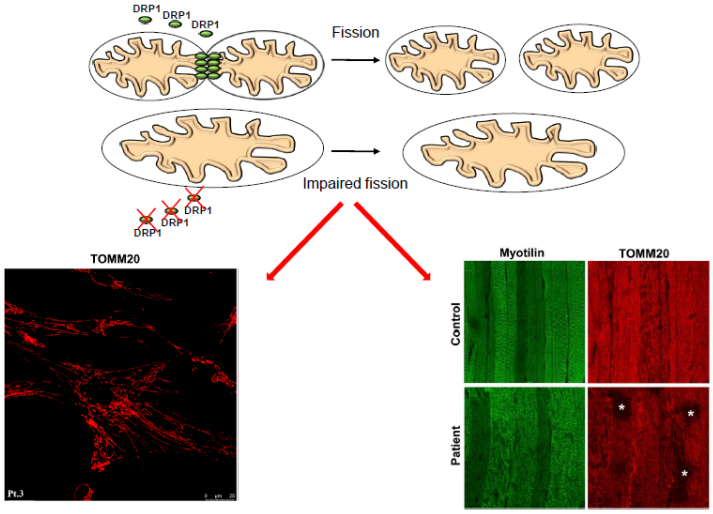

KEY WORDS: *DNM1L*; mitochondrial dynamics; mitochondrial fission; mitochondrial disorders; epileptic encephalopathy; muscle biopsy.

INTRODUCTION

The *DNM1L* (dynamin 1 like) gene encodes for the DRP1 protein, an evolutionary conserved member of the dynamin family, responsible for fission of mitochondria, a process required for normal mitochondrial dynamics and distribution. When activated, DRP1 translocates from a cytosolic pool to the outer mitochondrial membrane, where it oligomerizes, hydrolyzes GTP, and assembles into spiral filaments around mitochondrial tubules, allowing the organelles division. After the completion of this process, DRP1 spirals likely disassemble from mitochondria for future rounds of mitochondrial fission (Youle et al., 2012).

DRP1 has an important role in the maintenance of mitochondrial (Otsuga et al., 1998) and peroxisomal morphology (Pitts, 2004, Schrader et al., 2016), mediating organelle membrane remodeling during a variety of cellular processes. Mitochondria exist as a dynamic tubular network with projections that move, break, and reseal in response to

local environmental changes; the size and morphologic arrangement of mitochondria are due to a dynamic balance between mitofusins-dependent mitochondrial fusion and DRP1-dependent mitochondrial fission (Santel & Fuller, 2001).

Defects in mitochondrial dynamics, including the inhibition of mitochondrial fission and fusion, are responsible for many human diseases (Lenaers et al., 2012; Stuppia et al., 2015; Kim et al., 2017; Pozo Devoto & Falzone, 2017; Alexiou et al., 2017). Besides mutations in *DNM1L* (Waterham et al., 2007), dysfunctions in mitochondrial fission has been also associated with mutations in genes codifying for adaptors of DRP1, such as MFF and MID49/MIEF2 (Shamseldin et al., 2012; Koch et al., 2016; Bartsakoulia et al., 2018).

DRP1 impairment is implicated in several neurological disorders associated with either *de novo* dominant or compound heterozygous *DNM1L* mutations (MIM #603850). Encephalopathy due to defective mitochondrial and peroxisomal fission-1 is characterized by early onset with psychomotor delay and hypotonia, progressive course and death in childhood. Many patients develop refractory seizures, consistent with an epileptic encephalopathy, and thereafter show neurological decline. Age at onset, symptoms, and severity are variable, and some patients may not have clinical/biochemical evidence of mitochondrial or peroxisomal dysfunction (Fahrner et al., 2016; Nasca et al., 2016).

Better known clinical conditions that occur more frequently are related to defects in factors that conversely are implicated in mitochondrial membrane fusion such as Charcot–Marie–Tooth disease type 2A caused by dominant or recessive mutations in *MFN2* (mitofusin 2, MIM #608507), and optic atrophy or Leigh-like infantile encephalopathies caused by dominant or recessive mutations in *OPA1* (MIM #605290). Additional rare neurological phenotypes of “optic atrophy plus” syndrome and 3-methylglutaconic aciduria or cataracts are related to recessive or dominant mutations in *OPA3* (MIM #606580), a factor involved in mitochondrial shaping; a mild Charcot–Marie–Tooth disease type 2K is caused by biallelic recessive mutations in *GDAP1* (MIM #606598), that encodes for a mitochondrial protein involved in mitochondrial dynamics; and finally mitochondrial myopathy and ataxia has been recently reported to be due to dominant or recessive mutations in *MSTO1* (MIM #617619), encoding a cytoplasmic pro-mitochondrial fusion protein (Nasca et al., 2017).

Cultured fibroblasts from patients with these genetic conditions usually show either mitochondrial fragmentation, corresponding to genetic defects of factors implicated in mitochondrial membrane fusion (MFN2, OPA1) (Zanna et al., 2008), or abnormally elongated mitochondria and aberrant peroxisomes in cases with mutations in *MFF* (Koch et al., 2016) and *DNM1L* (Nasca et al., 2016).

Histochemical and ultrastructure characterization of skeletal muscle biopsies of subjects harboring *OPA1* mutations showed the presence of cytochrome c oxidase-deficient fibers associated with multiple mitochondrial DNA deletions in the majority of patients, either affected by dominant optic atrophy plus variants or with isolated optic nerve involvement (Yu-Wai-Man et al., 2010). On the other hand, few papers have reported studies on muscle biopsy of patients with mutations in additional genes regulating mitochondrial morphology, and no abnormalities have been found (Waterham et al., 2007; Fahrner et al., 2016; Yoon et al., 2016; Koch et al., 2016; Nasca et al., 2016), although Chao et al (2016) reported mitochondrial shape abnormalities at electron microscopy.

Here we describe on a series of 5 sporadic patients affected by severe epileptic encephalopathy associated with heterozygous mutations in *DMN1L* showing peculiar mitochondrial distribution changes in the muscle biopsy. So far, these abnormalities of mitochondrial distribution in muscle seem to be specific for the *DMN1L* related epileptic encephalopathy.

METHODS

Standard protocol approvals, registrations and patients consents

The study was approved by the Ethical Committees of the Bambino Gesù Children's Hospital, Rome, Italy, and the C. Besta Neurological Institute, Milan, Italy, in agreement with the Declaration of Helsinki.

Histological, ultrastructural and biochemical analyses in muscle

Cryostatic cross-sections of quadriceps muscle biopsies were processed according to standard histochemical and immunohistochemical procedures. Immunohistochemical studies were performed with rabbit polyclonal TOMM20 antibody (Santa Cruz Biotechnology) (in green) and with monoclonal antibody against merosin (Chemicon) (in

red). Confocal microscopy was performed on a Leica TCS-SP8X laser-scanning confocal microscope (Leica Microsystems, Mannheim, Germany) equipped with white light laser (WLL) source, 405nm diode laser, 3 Internal Spectral Detector Channels (PMT) and 2 Internal Spectral Detector Channels GaAsP. Sequential confocal images were acquired using a 63x-oil immersion objective (1.42 numerical aperture, Leica Microsystems) with a 1024x1024 format, and scan speed 400Hz. Z-reconstructions (30 stacks) were obtained with a z-step size of 0.3 μm. To improve contrast and resolution of mitochondrial distribution, confocal raw images were deconvolved by Hyvolution2 software (Leica Microsystems) before 3D reconstruction. Then deconvolved z-stacks were imported into LAS X 3D Analysis (Leica Microsystems) software to obtain their three-dimensional surface rendering. Each group of image was processed and analyzed using the same settings (i.e. laser power and detector amplification). For ultrastructural studies, muscle specimens were fixed in 2.5% glutaraldehyde in 0.1 M cacodylate buffer (pH 7.4) at 4°C. Samples were post-fixed with 2% OsO4 in 0.1 M cacodylate buffer (pH 7.4) for 1 h. Specimens were dehydrated in a graded series of ethanol and embedded in epon resin. Thin sections were evaluated with a transmission electron microscope (EM 109 Zeiss) (Fattori et al., 2018).

Respiratory chain complexes (RCCs) activities were assayed in muscle homogenate and normalized to citrate synthase activity, using a previously reported spectrophotometric method (Bugiani et al., 2004).

Mutational analysis

Genomic DNA was isolated from blood and cultured skin fibroblasts using QIAamp DNA mini kit (QIAGEN, Valencia, CA, USA). DNA from Pt.1, Pt.2 and Pt.3 underwent high-throughput sequencing by TruSight One panel (Illumina, San Diego, CA) comprehensive of > 4.800 clinically relevant genes. The enrichment was achieved following manufacture instruction and the sequencing analysis was performed on MiSeq System. Variant-Studio software was applied for analysis, classification, and reporting of genomic variants. After excluding previously annotated single nucleotide changes occurring with high frequency in populations (>1%), we prioritized variants predicted to have functional impact (i.e. nonsynonymous variants and changes affecting splice sites). Pt.4 and Pt.5 were analyzed using a custom gene panel for the screening of 224 genes associated with mitochondrial diseases (Ardissone et al., 2018). Sanger sequencing was

used to validate all the annotated functionally relevant variants, as well as to check variant segregation in the families. Bioinformatics tools based on heuristic methods, SIFT (http://sift.jcvi.org), PolyPhen-2 (http://genetics.bwh.harvard.edu/pph2) and Mutation Taster (http://www.mutationtaster.org/) were used for pathogenicity prediction of the variants**.**

For the identification of multiple deletions, we performed Long Range PCR using TaKara LA Taq DNA Polymerase (Takara Biotechnology-Dalian Co., Ltd.) amplifying a 11242bp mtDNA fragment with forward-4800 (5'ttcacttctgagtcccaga-3') and backward-16042 primers (5'ctgcttccccatgaaagagaacagagaa-3').

Western blotting analysis and antibodies

For SDS-PAGE, 40 μg of fibroblasts homogenate were loaded in a 12% denaturating gel. Western blot (WB) was achieved by transferring proteins onto polyvinylidene difluoride (PVDF) membrane and probed with specific antibodies. Specific bands were detected using Lite Ablot Extend Long Lasting Chemiluminescent Substrate (Euroclone, Pero (Mi), Italy). Densitometry analysis was performed using Quantity One software (BioRad, Hercules, CA, USA).

RCC subunits were detected using the following monoclonal antibodies purchased from MitoScience (Eugene, OR, USA): Complex I – NDUFA9; complex II – SDHB; complex IV – COXII; Complex V – ATP5B; porin (VDAC). Polyclonal rabbit GAPDH (Sigma-Aldrich) and monoclonal antibody OPA1 (BD Biosciences) and DRP1 (Abcam) were also used.

Biochemical analysis, Immunostaining and Imaging in fibroblasts

Human fibroblasts were obtained from a diagnostic skin biopsy and grown in DMEM medium supplemented with 10% fetal bovine serum, 4.5 g/L glucose, and 50 μg/mL uridine**.** Complex V activity (in the direction of ATP synthesis) was measured in fibroblast mitochondria, using reported spectrophotometric methods (Rizza et al., 2009). Mitochondrial respiration was measured using a SeaHorse FX-96 apparatus (Agilent Technologies, Santa Clara, CA), as previously described (Invernizzi et al., 2012).

To display the mitochondrial network arrangement, fibroblasts from Pt.1, Pt.2, Pt.3 were fixed and permeabilized using methanol:acetone (2:1) for 10 min at room temperature, then a blocking solution containing 5% BSA in PBS was used. The polyclonal rabbit

TOMM20 antibody (Santa Cruz Biotechnology) was applied overnight and visualized using Alexa Fluor 647 secondary antibody (Jackson ImmunoResearch), both antibodies were used at the dilution of 1:500. Images were acquired with a fluorescence-inverted microscope (Leica DMi8). An average of 8 image planes was obtained along the z-axis at 0.2 μm increments using LASX 3.0.4 (Leica) software. For Pt.4 and Pt.5 the mitochondrial network was visualized in living cells using the mitochondrial fluorescent dye MitoTracker Red-CMXRos (Invitrogen) at final concentrations of 50 nM for 30 min; then images were acquired with a confocal microscope (Leica TSC-SP8).

For peroxisomal immunostaining we used the polyclonal rabbit PMP70 antibody (Sigma-Aldrich) applied overnight at the concentation of 1:200, followed by Alexa Fluor 488 secondary antibody (1:500). The peroxisomal staining was visualized using the same parameters used above. Analysis of peroxisomal morphology was conducted using the image processing package ImageJ (Fiji). Images were then binarized, thresholded, and subjected to particle analysis to acquire form factor ("circularity": $4\pi^{*}\text{area/perimeter}^{2}$).

Functional studies in yeast

Yeast strains and media. The yeast strains used in this work were the haploid strain W303-1B (*MATa leu2-3, trp1-1, can1-100, ura3-1, ade 2-1, his3-11*) and its isogenic strain *dnm1*::KanR, and the hemizygous diploid strain W303 *dnm1Δ* (*MATa*/*MAT**a*** *leu2-3/leu2-3, trp1-1/trp1-1, can1-100/can1-100, ura3-1/ura3-1, ade 2-1/ade2-1, his3-11/his3-11 DNM1/dnm1*::KanR). All experiments were performed in Synthetic complete medium (SC, 6.9 g/l yeast nitrogen base without amino acids (ForMedium), 1 g/l drop-out mix without amino acids or bases necessary to keep plasmids) (Kaiser et al., 1994). Media were supplemented with carbon sources (Carlo Erba Reagents) as indicated in the text in liquid phase or after solidification with 20g/L agar (ForMedium).

Construction of *dnm1* mutant strains. *dnm1* mutant alleles and *dnm1* mutant strains were constructed as previously reported (Nasca et al., 2016). Briefly, *dnm1* mutant alleles were constructed using mutagenic overlap PCR with the oligonucleotides reported in Supplementary Table S1, digested with *Bam*HI and *Xba*I or *Xba*I and *Sal*I, and subcloned in pFL38DNM1. In order to obtain haploid wild type or mutant strains all plasmids were introduced by transformation in the W303-1B *dnm1Δ* haploid strain and in the W303

dnm1Δ hemizygous diploid strain using the "LiAc/SS carrier DNA/PEG quick method" as previously reported (Gietz & Woods, 2002).

Yeast analyses. Spot assay was performed by spotting $5x10^4$, $5x10^3$, $5x10^2$ and $5x10^1$ cells on SC supplemented with different carbon sources. *Petite* frequency was measured as previously reported (Baruffini et al., 2010) in six to eight independent clones for each strain. Oxygen consumption rate was measured in SC medium as previously described (Goffrini et al., 2009) on five independent clones, after growth in conditions, which minimized the *petite* frequency, which was lower than 5%. (Nolli et al., 2015). All experiments were performed at 37°C, except for the measurement of the *petite* frequency in the diploid strains, which was performed at 28°C.

Statistical analysis

For each experiment, data obtained were calculated as the mean of replicates ± standard deviation (SD). For analysis on peroxisomal morphology data were analysed using unpaired two-tailed Student's *t*-tests; for yeast experiments, data were compared with one-way ANOVA followed by Bonferroni's test.

Structural analysis

The residues affected by the missense mutations described in this work (p.Gly223Val, p.Gly362Asp, p.Phe370Cys, and p.Arg403Cys) were mapped on crystal structures of homologues proteins. The crystal structure of a dimeric human dynamin-1-like protein (Protein Data Bank, PDB, 3W6O) was used for the p.Gly223Val mutation. The crystal structure of the Dynamin-3 tetramer (PDB 5A3F) was used for the p.Gly362Asp, p.Phe370Cys, and p.Arg403Cys mutations. The cryo-electron microscopy structure of human dynamin-1 co-assembled with MID49 (PDB 5WP9) was used to obtain the detailed view of the site of the p.Phe370Cys mutation. Molecular structures were rendered with PyMOL (http://www.pymol.org).

RESULTS

Clinical features and Brain MRI findings

Patient 1 is a girl single-born from unrelated healthy young parents. At birth, there was no breathing distress, no jaundice, and weight was 2.850 kg. She had normal motor milestones in the first year of life and was able to walk without any support at age 17 months. She pronounced her first words around 1 year of age, and later at age 4 years she started in kindergarten and had good attendance and integration. At age 2 years and a half, the child manifested generalized clonic seizures while falling asleep, and then displayed an ataxic syndrome with prominent intentional and postural tremor that persisted for 2 weeks. About 7-8 weeks later, a cluster of myoclonic seizures of face and left side limbs with vomiting and drooling appeared together with relapsing of ataxia. She was admitted at a local hospital were a brain MRI showed T2 hyperintensities in the posterior white matter regions and some T2 hyperintensities in the cortical areas. More recently, a MRI performed at age 6 years showed moderate global cerebral and cerebellar atrophy (Figure 1A-B and E-F). Serial MRIs taken in the same month at different days showed that the cortical DTW restriction hyperintensity in the right precentral gyrus and in the pallidum and thalamus of the right hemisphere (Figure 1C) spontaneously vanished 20 days later when a serial brain MRI was performed (Figure 1D). She was admitted at our hospital for a Super refractory Status Epilepticus (SRSE) which began one month before, and was unresponsive to multiple doses of tiopentone. SRSE was treated with propofol and with high dose of topiramate and perampanel, and was characterized by repetitive to continuous focal myoclonic seizures clinically lateralized to the right side, especially involving the face and the right arm. The polymyographic video/EEG recordings showed high amplitude theta-delta activity, lateralized to the left side. Ictal EEG confirmed the cortical nature of the seizures as it was characterized by low amplitude rhythmic fast discharge lateralized to the left side evolving into a focal spike-and-wave complexes, corresponding to the clinical focal contralateral myoclonus. Intercritical EEG confirmed the interhemispheric asymmetry with persistent slow activity over the left central regions. SRSE lasted for 50 days and was the only status epilepticus she had so far.

Patient 2 is a boy born as a preterm infant from TC scheduled at 36 weeks of gestational age because prenatal ultrasound monitoring indicated a fetal growth restriction appearing

in the last trimester. At birth weight was 2.020 kg, Apgar 9-10. The neonatal period was uneventful, and developmental milestones were regular because he started to walk without support at the age 15 months, although he showed delay in attaining language and failure to thrive (weight always around 3rd centile) from the first months of life. Preliminary genetic investigations (karyotype, MLPA 22q12.2, telomeres, fragile X) yielded no abnormalities. Moreover, gastroenterological and endocrinological investigations (FT4, TSH, IgA, EMA, Anti TG, AGA) carried out during hospitalization showed increased GOT (84.9 IU/L), central hypothyroidism (TSH levels 1.27 mU / ML, Ft3 2.4 pg/ml with NV of 2.4-4.2 and Ft4 7.6 pg/ml with NV of 8.5-16.5) and low levels of ACTH (18 pg/ml with NV of 0-46 pg/ml). During the follow up increased serum lactate was detected (4.71 mmol/l, NV 0.6-2.3 mmol/l). The child was treated with thyroid hormone and started therapy with hydrocortisone. Around age 3 years the boy started with a prolonged repetitive left hemiclonic SRSE and additional single episodes relapsed during the follow-up with a frequency of at least twice a month although he was taking antiepileptic polytherapy with phenobarbital, topiramate, and clonazepam. At age 7 years serial brain MRIs performed three times in a timeframe of 3 months, showed only a slight global cerebral atrophy, and a cortical DTW restriction hyperintensity was observed only once in the right precentral gyrus (Figure 1 G-J). MR spectroscopy did not detect any lactate peek. Polymyographic video/EEG recordings during one episode of SRSE with subsequent left focal myoclonic seizures, showed, only as a counterpart of the seizures, a pattern of RHADs (Rhythmic High Amplitude Delta superimposed by fast activity) over the contralateral central regions. Focal RHADs were also present during sedation. Later on, during the SRSE, which was treated with topiramate, propofol and ketamine, RHADs were no longer recorded, and were replaced by persistent focal slow activity. SRSE lasted 17 days together with epilepsia partialis that was noticed over the left side of the body.

Patient 3. The girl is the second child from unrelated parents; an eldest sister aged 12 years was healthy. She was born by a planned TC delivery, at term, and weight was 2.950 kg at 40 weeks of gestation. The child had a normal development from the newborn period to the age of 5 years, although a mild hearing loss was suspected. Around the age of 5 years she was admitted to the intensive care for the abrupt manifestation of a myoclonic status epiplepticus during an intercurrent febrile episode. The patient needed a prolonged hospital admission because she manifested repeated

severe myoclonic or right prolonged hemiclonic SRSE that was associated with a psychomotor deterioration. During the follow up the child presented with very frequent and long duration seizures of generalized or hemiclonic SRSE and a persistent interictal myoclonus at upper and lower limbs. One previous brain MRI performed at age 3 years was considered normal, while the last brain MRI performed at age 7 years (Figure 2A-D) showed global cortical atrophy that was prominent in both the right hemisphere and the homolateral cerebral peduncle. There was also abnormal T2 high intensity signal (long TR images) of the deep white substance at the semi-oval white matter and in the paratrigonal site bilaterally with involvement of the subcortical spaces in the temporo-insular areas bilaterally (data not shown). The DWI study did not show any signs of recent cerebral and cerebellar parenchymal abnormalities. The ventricular system was moderately enlarged. Polygraphic video/EEG recordings performed during the chronic phase of the disease showed poorly organized cerebral activity, both in wakefulness and sleep, with theta activity superimposed by fast rhythms. Polymyographic recording confirmed right side high frequency myoclonus, predominantly at the right hand and right face, rhythmic in nature, persistent during sleep, without a clear-cut correlation with the EEG transients.

Patient 4 is the only child from unrelated parents. A half-brother from previously mother's marriage presented with severe psychomotor delay, refractory epilepsy and myoclonic status epilepticus at 2 years of age; he died for unknown reason at 3 years. This boy was born at term after an uncomplicated pregnancy and delivery. Psychomotor delay was reported since the first months of life: he achieved sitting position at 12 months, autonomous gait and first words at 3 years of age. First neurological evaluation performed at 4 years showed psychomotor delay and pyramidal signs at lower limbs; instrumental exams including brain MRI and EEG were reportedly normal. At 5 years and 5 months of age, few days after a viral illness, he presented partial motor status epilepticus. In the following months, refractory epilepsy and psychomotor regression were reported. He manifested motor partial, tonic, myoclonic seizures and spasms, and experienced two episodes of myoclonic status epilepticus resembling SRSE, refractory to midazolam, thiopentone, vitamin B6 and propofol. EEGs were not available; brain MRI performed one month after first status epilepticus disclosed T2 hyperintensities in thalami and in right hemisphere temporo-parieto-occipital cortex that appeared reduced 40 days later when a serial brain MRI was performed (Suppl. Figure S1 A-E). He was

admitted to our hospital at 5 years and 9 months manifesting spastic tetraparesis, no postural control, hyperkinesis but poor voluntary movements and severe cognitive impairment. Seizures frequency was daily. Polymyographic video/EEG disclosed epilepsia partialis continua at the right arm intermingled with asymmetric tonic seizures mainly involving left side arm and related with generalized low voltage fast rhythms with parieto-occipital prevalence, EEG background activity and sleep pattern were not organized. Brain MRI showed global cerebral atrophy (Suppl. Figure S1 F-J). Visual and sensory evoked potential showed central conduction abnormalities, motor and sensory nerve conduction velocities disclosed sensitive and motor axonal neuropathy. Fundus oculi and brainstem auditory evoked were normal. Blood routine exams, pyruvate, amino acids plasmatic levels, very long chain fatty acid (VLCFA), phytanic acid and urinary organic acids were normal. Mild elevated lactate level in serum was detected (2.3 mmol/l nv 0.8-2.1). Respiratory chain complexes activity was normal in muscle. Patient died for respiratory failure at 6 years of age.

Patient 5 is the only child from unrelated parents. Family history was unremarkable. She was born at term after an uneventful pregnancy. At birth weight was 3.050 kg, Apgar 9-9. After birth, she presented respiratory distress that required intensive care and oxygen supplementation for 20 days. During the first months, psychomotor development was reportedly normal (head control at 2 months of age). Between 4-6 months of age development delay and failure to thrive became evident; from 7-8 months to 1 years of age she suffered from self-inflicted finger and mouth ulcers and pain insensitivity was reported (i.e. receiving vaccine injections). In the second year of life she presented prolonged clonic seizures at left face. At 3 years of age she was first evaluated in our institute: she presented with short stature (weight and length <3rd percentile), microcephaly (<3rd percentile), dysphagia, tetraparesis with extrapyramidal signs, dystonic postures involving both upper and lower limbs, dyskinesias and athetoid movements, absence of postural control, absence of language. Epileptic seizures were not noticed from parents but polymyographic video/EEG recorded tonic seizures at upper limbs related with multifocal generalized epileptiform abnormalities and showed poorly organized cerebral activity, both in wakefulness and sleep. Treatment with leveretiracetam was started but EEG pattern remained unchanged. From the age of 4 years dyskinesias and dystonia worsened. Serial bran MRI (7 months 2 ys and 1 month, 4 ys and 4 months) showed thin corpus callosum together with signs of increased cortical

subarachnoid spaces suggesting cortical involvement, and progressive cerebellar atrophy (Suppl. Figure S2); no cortex involvement was noticed. Brainstem auditory evoked and visual evoked potential showed central conduction abnormalities, motor and sensory nerve conduction velocities disclosed sensitive and motor axonal neuropathy. Fundus oculi was normal. Blood routine exams, plasmatic uric acid, lactate and pyruvate in plasma and CFS, plasmatic amino acids levels, VLCFA were normal. Molecular analysis of *PLA2G6, POLG1*, NARP/MILS mutations were negative. Muscle biopsy was not performed. At last follow up, at 5 ys, clinical conditions were stable.

Histological and biochemical analyses

Histochemistry of the muscle sample of Pt.1, Pt.2, Pt.3 showed scattered fibers with a patchy reduction of cytochrome *c* oxidase (COX) and succinate dehydrogenase (SDH) stain with aspects of polymorphic core like areas (Figure 3, left and central panels). Similarly areas of reduced immunoreactivity were observed using the TOMM20 antibody confirming impairment of the mitochondrial network distribution (Figure 3, right panel). Muscle histochemistry in Pt.4 also showed multiple areas of patchy reduction of cytochrome *c* oxidase (Suppl. Figure S3 A), while Electron Microscopy (EM) showed enlarged mitochondria; sometimes two mitochondria were coupled and appeared to be in close relationship to each other (Suppl. Figure S3 B-C). Occasionally, the sarcomeric organization appeared to be normal, though the Z line was often absent (Suppl. Figure S3 D). In addition, in some areas mitochondria were quite absent (Suppl S3 Fig E-F), whereas in others they were present in large collections (Suppl S3 Fig G-H). Histochemical serial sections of the muscle biopsy in Pt. 3 showed that fibers devoid of mitochondria were type 1 fibers (Supp. Figure S4). Furthermore, confocal microscopy of the muscle biopsy (Supp. Figure S5, Supp. Figure S6) showed an altered and irregular array of Z-bands, while patchy areas devoid of mitochondria were clearly observed with TOM20 staining. In spite of the irregular aspect of the Z bands in confocal microscopy, no major alterations such as streaming of the Z bands were observed at the EM level (Supp. Figure S3).

Histochemistry of the muscle sample of a patient harboring compound heterozygous mutations in *OPA1* (Nasca et al., 2017) was studied and compared with those of *DNM1L* patients and showed no patchy staining abnormalities (Figure 3 lowest panel). In addition, by Long Range PCR we also searched comparatively for multiple deletions in

muscle samples and found multiple deletions only in the *OPA1* mutated patient and no in the *DNM1L* patients (data not shown).

Muscle biopsy was not performed in Pt.5.

RCCs biochemical analysis in muscle homogenate was normal in all patients (data not shown). Accordingly, the activity of Complex V (in the direction of synthesis of ATP) measured in Pt.1 fibroblast mitochondria, as well the oxygen consumption in Pt.4 and Pt.5 fibroblasts were normal (data not shown).

Mutational analysis

Bioinformatics analysis carried out on the TruSight One panel, performed in Pt.1, Pt.2 and Pt.3, led to the identification of a single gene entry, *DNM1L* (NM_012062, NP_036192). In Pt.1 we identified the heterozygous, previously unreported variant c.668G>T (p.Gly223Val) (Figure 4A); in Pt.2 we identified the heterozygous variant c.1207C>T (p.Arg403Cys), already reported (Fahrner et al., 2016) (Figure 4B); in Pt.3 we identified the heterozygous unreported variant c.1109T>G (p.Phe370Cys) (Figure 4C). Segregation for the three mutations in the corresponding families was negative, and then they can be considered as *de novo* mutations. Similar filtering analysis was applied to the panel, containing ~230 genes associated with mitochondrial disease, used for Pt.4 and Pt.5. In Pt.4 we identified 2 heterozygous *DNM1L* variants: c.1085G>A (p.Gly362Asp) and c.1535T>C (p.Ile512Thr) (Figure 4D-D'). The first nucleotide change corresponded to rs148686457, with a frequency 0.008% in the ExAC database, whereas the second was not reported in any public database. Given that *DNM1L* mutations may present as recessive or dominant traits, we evaluated the segregation in the healthy parents of Pt.4 by Sanger sequencing: we found that the c.1535T>C (p.Ile512Thr) was inherited from the mother (Figure 4D') while the c.1085G>A (p.Gly362Asp) was not present in any of the two parents and may represent a *de novo* event (Figure 4D). Indeed, the same change has been recently reported as a *de novo* mutation (Vanstone et al., 2016). An in-depth evaluation of the familial history revealed that the mother had a son with epileptic encephalopathy from another man. This child died at 3 years of age: no material was available for genetic studies. By subcloning PCR products obtained from Pt.4's cDNA, we were able to assess that the two *DNM1L* variants were on the same allele (i.e., the maternal allele, harboring the c.1535T>C

variant identified in the mother). Moreover, a further analysis of *DNM1L* genomic region using a next-generation sequencing (NGS) approach revealed that the c.1085G>A was present in the mother's blood DNA, although at very low level (~5%). These findings suggested a maternal germline mosaicism for the dominant mutation c.1085G>A (p.Gly362Asp), that may even explain the affected status of the Pt.4's half-brother (Suppl. Figure S7). In Pt.5 we identified a heterozygous variant c.1084G>A (p.Gly362Ser); the variant was not detected in the parents' DNA by Sanger or NGS analyses (Figure 4E). The variant was absent in public SNP databases; nevertheless, it was reported as a *de novo* mutation in a patient with refractory epilepsy (Sheffer et al., 2015).

All new mutations herein reported were pathogenetic while tested *in silico* (Suppl. Table S2), and were not reported in public (dbSNP142, ExAC, 1000 Genomes, HGMD, gnomAD) and in-house databases.

Western blotting analysis

To evaluate the impact of the mutations on DRP1 stability, we performed WB analysis on fibroblasts. We observed a significantly increased (in Pt.3) or normal (in Pt.1, Pt.2, Pt.4 and Pt.5) level of the protein when normalized to GAPDH (Figure 5A-B), in contrast with the strong reduction present in *DNM1L*-recessive cases (Nasca et al., 2016). The expression level of OPA1 and of different subunits of the RCCs showed no differences compared to controls (data not shown).

Immunostaining and imaging in cultured fibroblasts

Because of the pivotal role of DRP1 on dynamics of mitochondria and peroxisomes, we performed morphological studies on patients' fibroblasts. We used the antibody TOMM20 in fixed cells (for Pt.1, Pt.2 and Pt.3) or Mitotracker red in living cells (for Pt.4 and Pt.5), both specific for mitochondrial staining. In normal glucose medium we observed an increased filamentous network in mutant fibroblasts of all patients (Suppl. Figure S8, left panels), although Pt.1 displayed a mixed population in which hyperfused mitochondria are associated with swollen and rod-shaped mitochondria and Pt.5 showed dot-shaped mitochondria (Figure 6, left panel). In galactose-supplemented medium, a condition that forces cells to use the oxidative phosphorylation for ATP production and usually causes elongation of mitochondrial network in control cells, the mitochondrial

network of *DNM1L*-mutant fibroblasts showed a lower tendency to fuse associated with a more disorganized network and an altered mitochondria morphology, with swollen, dots, rings, and "chain-like" structures (Figure 6, right panels; Suppl. Figure S8 right panels).

For the immunovisualization of peroxisomes, we used an antibody against a peroxisomal protein, PMP70. In contrast with the highly diffused punctuated staining present in control cells, in Pt.4 and Pt.5 cytoplasm (Figure 7) we observed organelles longer, larger, and less uniformly distributed into cytoplasm; although in minor extent, peroxisomal alterations were present also in Pt.1, Pt.2 and Pt.3 (Suppl. Figure S9). Accordingly, the morphometric analysis showed decreased form factors for circularity in the patient's cells compared to controls, with a significant reduction for Pt.4 and Pt.5 (Figure 7; Supp. Figure S9).

Functional studies in yeast

The deleterious effect of the p.Arg403Cys substitution was already experimentally demonstrated (Fahrner et al. 2016). To assess the pathogenic role of the other identified *DNM1L* variants as well as to compare the effects of different substitutions on the same amino acid (p.Gly362), we performed complementation studies in a *S. cerevisiae* strain lacking *DNM1,* hereafter referred to as *Δdnm1*. *DNM1* is the yeast orthologue of human *DNM1L;* the amino acid residues corresponding to p.Gly223Val, p.Gly362Asp, p.Gly362Ser and p.Ile512Thr variants are conserved between the two species, being in yeast p.Gly252, p.Gly397, p.Ile543, whereas human p.Phe370 is not conserved, being p.Tyr405 in yeast. The *dnm1*Δ strain was transformed either with the wt *DNM1*, the $dnm1^{G252V}$, $dnm1^{G397D}$, $dnm1^{G397S}$or $dnm1^{I543T}$ mutant alleles, under the endogenous *DNM1* promoter, as well as with the empty plasmid. To test the possible effects on mitochondrial function, we first evaluated the oxidative growth by spot assay analysis on medium supplemented with either glucose or ethanol or glycerol. The oxidative growth of the $dnm1^{G397D}$ and the $dnm1^{G397S}$ mutant strains was partially affected compared to the *DNM1* wild type strain, especially on ethanol, whereas the growth of the $dnm1^{G252V}$ was similar to the strain *dnm1Δ*; on the contrary the growth of the $dnmI^{I543T}$ mutant was unaffected (Figure 8A). To further investigate the OXPHOS defect, the oxygen consumption was measured and according to the growth phenotype, the oxygen consumption rate of the $dnm1^{G397D}$ and of the $dnm1^{G397S}$ mutants was respectively 30% and 20% lower than that of the wild type strain, whereas the oxygen consumption rate of

dnm1^{G252V} and of the *dnm1* null strain was decreased by 60%; also the *dnmI*^{I543T} mutant showed a slight though significant reduction of respiratory activity (Figure 8B). In yeast, mutations in several nuclear genes encoding for proteins involved in mitochondrial dynamics, such as *MGM1* (the homologous gene of human *OPA1*), (Sesaki et al., 2003; Nolli et al., 2015), *FZO1* (h*MFN1*), (Rapaport et al., 1998) and *DNM1* itself (Bernhardt et al., 2015), affect mtDNA stability. Although the patients reported in this study did not show any mtDNA defects, we measured the frequency of *petite*, i.e. clones which are unable to grow on an oxidative carbon source due to large deletions or lack of mtDNA, in order to further highlight the defect of mutant Dnm1 proteins. Deletion of *DNM1* as well as the expression of *dnm1*^{G252V} resulted in a significant increase of *petite* frequency (~50%) compared to the wild-type strain, whereas expression of *dnm1*^{G397D} or *dnm1*^{G397S} partially decreased mtDNA stability (~40% and ~25%, respectively), which is, however, lower than the *DNM1* wild-type strain or the *dnmI*^{I543T} (~8% and ~15%, respectively) (Figure 8C).

Altogether these results validated the pathogenicity of the mutations Gly252Val, Gly397Asp and Gly397Ser, showing also that substitution of Gly397 with aspartate is more deleterious than substitution with serine. The amino acid change Ile543Thr slightly affects the activity of the protein as well, being the respiratory activity and the *petite* frequency slightly altered compared to *DNM1* wild type. Since the variant Ile512Thr was present in the patient in *cis* with the Gly362Asp, we also constructed a yeast mutant allele carrying both the corresponding variants. Interestingly, the *dnm1*$^{G397D\text{-}I543T}$ strain showed a more severe phenotype than the strain carrying the sole mutation Gly397Asp; in fact, the oxidative growth, the respiratory activity and the mtDNA mutability become similar to that of the null mutant suggesting that Ile543Thr is a phenotypic modifier (Figure 8A-C).

Finally, we tested whether the mutations have a dominant or recessive effect by measuring the oxygen consumption rate of the diploid hemizygous *DNM1*/*dnm1Δ* strain transformed with the plasmid having mutant alleles or with the empty vector. The respiratory activity of the heteroallelic strains *DNM1*/*dnm1*^{G397D}, *DNM1*/*dnm1*^{G397S} and *DNM1*/*dnm1*$^{G397D\text{-}I543T}$, but not that of *DNM1*/*dnm1*^{G252V} and *DNM1*/*dnm1*^{I543T}, was lower compared to the hemizygous strain *DNM1*/*dnm1Δ*. This indicates that Gly397Asp and Gly397Ser have a partial dominant-negative effect whereas Ile543Thr and, quite

unexpectedly, Gly252Val act as recessive mutations (Figure 8D), at best concerning the effect on oxygen consumption. To better deepen this point, we investigated in the heteroallelic strain *DNM1*/*dnm1*^{G252V} another phenotype, i.e the *petite* frequency, based on the observation that the mutation Lys41Ala, generally recognized as dominant (Frank et al., 2001), increased the *petite* frequency in an heteroallelic diploid mutant strain (Nasca et al., 2016). The significant increase (3.3-fold±0.6, $p<0.001$) of the *petite* frequency observed, compared to the hemizygous strain, suggests that also the Gly252Val mutation behaves as partially dominant, at least for this specific phenotype.

Structural analysis

All the identified missense mutations affect sites, which are totally or highly conserved sites among species (Figure 9A) and imply replacements with residues presenting physicochemical properties that differ significantly from those of the wild type amino acids. The p.Gly223Val mutation causes the substitution of the tiny and flexible glycine with a hydrophobic valine, which is expected to induce structural changes in the GTPase domain near residues 215-221 important for the binding of GTP (Figure 9B). The p.Gly362Asp and p.Gly362Ser mutations replace the tiny glycine with the anionic aspartic acid or with the hydrophilic serine, respectively, modifying the N-terminus of an α-helix also exploited in dynamin tetramerization (Figure 9C), as inferred by homology of dynamin-1-like with dynamin 3, another member of the dynamin family. The p.Phe370Cys mutation affects the large and hydrophobic phenylalanine that is important for the stability of monomers and for the tetramer formation (Figure 9D). In fact, Phe370 is involved in several intramolecular hydrophobic interactions, which are disrupted by the replacement with the small cysteine and the latter might also become engaged in disulfide bond formation with other cysteines located nearby (Suppl. Figure S10). The p.Arg403Cys mutation implies the change of the cationic arginine into the tiny and neutral cysteine at sites that contribute to the core of tetrameric dynamin assembly (Figure 9E), as previously reported (Fahrner et al., 2016).

DISCUSSION

Here we described five patients with epileptic encephalopathy and *de novo* dominant missense mutations in *DNM1L*. We identified two novel variants in Pt.1 and Pt.3, whereas in Pt.2 and Pt.5 we found two variants that were reported so far (Fahrner et al., 2016; Sheffer et al., 2015). Pt.4 showed two variants on the same allele; the first was inherited from the mother and the second, recently described as a *de novo* mutation (Vanstone et al., 2016), was present in the mother's blood DNA at low level (~5%), suggesting a maternal mosaicism. We observed a quite strict genotype-phenotype correlation, with overlapping clinical presentations between Pt. 2, Pt. 4, Pt. 5 and the previously described patients harboring the same mutation (reported by Fahrner et al., 2016, Vanstone et al., 2016 and Sheffer et al., 2015 respectively).

Following the first description of Waterham et al. (2007), there have been increasing reports in the last 2 years on patients, frequently sporadic, with *de novo* dominant-negative *DNM1L* mutations who are affected by early onset encephalopathy with microcephaly and drug resistant seizures, progressive brain atrophy or abnormal brain development, optic atrophy, and occasionally persistent lactic acidemia. The degree of severity was broad, ranging from neonatal death to prolonged survival (Fahrner et al., 2016; Zaha et al., 2016; Sheffer et al., 2016; Vanstone et al., 2016; Chao et al., 2016). A similar spectrum of clinical presentations has been also reported for *DNM1L* recessive mutations (Yoon et al., 2016; Nasca et al., 2016). More recently, dominant mutations in *DNM1L* have been also related to isolated optic atrophy in three large families (Gerber et al., 2017).

The patients described here presented clinical manifestations quite similar to previously reported *DNM1L* cases manifesting early onset encephalopathy and characterized by development delay, together with episodes of SRSE, progressive cerebral atrophy, and transitory abnormal T2 hyperintensities and DTI restriction areas at MRI. In addition, elevated lactate level in serum was detected in Pt.2 and Pt.4, whereas lactate was normal in other patients. There are no clues about a peroxisomal dysfunction: when available (Pts 4 and 5), plasma phytanic and pristanic acids concentrations, typically increased in patients with peroxisomal disorders [ten Brink et al., 1992], were normal. Excluding the 16 patients with mild non-syndromic optic atrophy, six patients of the twelve reported in literature showing similar clinical manifestations died in early-childhood (Waterham et

al., 2007; Chao et al., 2016; Yoon et al., 2016; Zaha et al., 2016) and in four cases death occurred in the first year of age (Waterham et al., 2007; Chao et al., 2016; Yoon et al., 2016). It is not clear why some mutations give rise to premature death. The cause of the early-childhood death cannot be attributed to the mode of transmission, since early death occurred both in patients with a dominant *de novo* mutation and in patients with recessive mutations (Waterham et al., 2007; Chao et al., 2016; Yoon et al., 2016; Zaha et al., 2016), neither to the residual amount of DRP1, given that fibroblasts from a patient with long survival showed a strong reduction of the total amount of the protein (Nasca et al., 2016). In the cohort of our patients only the Pt.4 died at six years of age, differently from the one already described with the same p.Gly362Asp mutation who showed prolonged survival (Vanstone et al., 2016). However, Pt.4 carried also a second, maternally inherited heterozygous *DNM1L* variant (p.Ile512Thr), which may explain the different degree of severity in these two cases; indeed, the yeast studies suggested that the p.Ile512Thr change can be a modifier, able to worsen the phenotype associated with the p.Gly362Asp mutation.

Clinical signs of a severe epileptic encephalopathy with frequent episodes of SRSE and EEG abnormalities do not seem to be peculiar signs of this condition. Noteworthy, MRI abnormalities, and particularly the detection of transitory abnormal T2 hyperintensities and DTI restriction areas in the basal ganglia or the cortical areas are quite characteristic for *DNM1L* encephalopathy, although may rarely occur in other conditions such as MELAS or may represent a unspecific sign due to status epilepticus.

Probably the most peculiar finding in the cohort of our patients is the muscle histology/histochemistry showing core like areas using oxidative enzyme staining for COX and SDH, which suggest an abnormal distribution of mitochondria in the muscle tissue. We found this pattern in all the examined muscle biopsies. Notably, reduced mitochondrial numbers and size and a paucity of mitochondria between sarcomeres in muscle have been noticed in transgenic Drosophila models expressing *DNM1L* variants identified in patients (Chao et al., 2016). Areas devoted of mitochondria have not been found in muscle biopsies of *OPA1* mutated patients that can sometimes show ragged red-COX negative fibers correlated with mitochondrial DNA instability (Amati-Bonneau et al., 2008). In the investigated patient with recessive OPA1 defect, although COX negative fibers were not detected, we confirmed multiple deletions. Contrariwise, in

muscle samples of *DNM1L* patients, the impairment of the mitochondrial network distribution was not associated with mitochondrial DNA instability.

The primary sequence of DRP1 consists of four conserved regions: the GTPase domain, the middle, the variable, and the GTPase effector domain (GED). Revising all the cases published, we noted that mutations that fall into the GTPase domain are typically associated with a recessive trait (except for the cases not associated with early encephalopathy, reported by Gerber et al., 2017), while mutations that fall into the middle domain are expressed as dominant-negative. Here, we report on four mutations falling in the middle domain, which we suggest having a dominant negative effect on the oligomers stability. In fact, we likely exclude a DRP1 haploinsufficiency, as we observed normal or significant increase of protein level by western blotting analysis. Moreover, we excluded a gain of function effect on the physiological activity of DRP1 because we did not observe increase in mitochondrial fission; on the contrary patient' fibroblasts showed hyperfused mitochondria. In only one of our patients (Pt. 1) we identified a mutation (p.Gly223Val) which falls into the GTPase domain, even if the nucleotide change is located at the boundary between the GTPase and the central domain. The yeast model indicated that it acts with a dominant-negative effect but probably through a mechanism different from the other mutations located in the middle domain. It is possible that the same mechanism may explain also the cases with isolated optic atrophy, harboring dominant mutations in the GTPase domain (Gerber et al., 2017); nevertheless, a gain of function effect has been postulated as well (Wangler et al., 2018).

In the cytosol, DRP1 exists as a mixture of dimers and tetramers (Macdonald et al., 2014) and, when recruited to mitochondria via receptors anchored to the mitochondrial outer membrane (Losón et al., 2013), hydrolysis of GTP triggers conformational changes in DRP1 oligomers that generate the mechanical force to promote mitochondrial membrane scission (Francy et al., 2015). The middle and GED domains promote DRP1 self-assembly, required for mitochondrial fission (Chang et al., 2010), while the variable domain seems to act as a negative regulator of DRP1 self-assembly (Francy et al., 2015).

Structural analysis revealed hypothetical mechanisms of protein impairment and malfunctioning for all the missense mutations presented in this study. Specifically, the p.Gly223Val substitution seems to hamper the binding of GTP, hence the GTPase activity, the p.Gly362Asp mutation impairs the tetramer formation, as previously

described by the two-hybrid experiment of Farhner et al., 2016. Finally, also the p.Phe370Cys could influence the protein oligomerization. In the patient fibroblasts with this mutation we observed a significant increase of DRP1 level probably due to its altered degradation, in fact this amino acid change might cause disulfide-mediated abnormal multimerization. As matter of fact, in the protein structure the p.Phe370Cys mutation is located close to the mouse p.Cys452Phe substitution (p.Cys446Phe in the human protein), which has been demonstrated to cause an increase in higher-ordered assembly with supranormal GTPase function and a failure of oligomer disassembly (Cahill et al., 2016).

At the cellular level we found the presence of hyperfused, swollen and rod-shaped mitochondria in fibroblasts from all our patients, as reported for others *DNM1L* mutations (Waterham et al., 2007, Fahrner et al., 2016; Zaha et al., 2016; Sheffer et al., 2016; Vanstone et al., 2016; Nasca et al., 2016; Gerber et al., 2017; Ladds et al., 2018; Ryan et al., 2018). The morphological anomalies were not associated with overt OXPHOS dysfunctions, in fact we did not observe reduction of OXPHOS subunits levels and cellular respiration was unaffected. Likewise, the activities of the MRC complexes in muscle were normal in the four patients of our cohort for whom muscle biopsy was obtained. The same findings have been reported in most of the *DNM1L*-mutant cases; in only few patients slightly decreased activity of complex IV, altered ATP production or impaired oxygen consumption were observed in fibroblasts (Sheffer et al., 2016; Nasca et al., 2016), or in muscle (Ladds et al., 2018). Surprisingly, histochemistry of Pt.1, Pt.2, Pt.3 and Pt.4 showed scattered fibers with a partial reduction of COX and SDH stainings, and with aspects of polymorphic core like areas. Moreover, we also identified areas with reduced immunoreactivity to mitochondrial signal, suggesting an abnormal distribution of organelles. Accordingly, the EM examination showed a few fields, mainly located at the center of the fibers, devoid of mitochondria. In these areas the sarcomeric organization was quite normal, though the Z lines were often absent (Supp. Figure S3) as reported in selenoprotein-related diseases (Cagliani et al., 2011), or somewhat irregular (Supp. Figure S5, Supp. Figure S6). Interestingly, at EM the areas devoid of mitochondria did not show any major misalignment such as streaming of the Z-bands, that is well known to occur in the cores which are typically devoid of oxidative stains in RYR1 related myopathies (Monnier et al; 2000). This is a new finding and can be considered as a key aspect suggesting mutations in *DNM1L*. In fact, no peculiar

histochemical alterations have been reported so far in the muscle biopsies of *DNM1L* patients. The histological features of muscle biopsies associated with the *de novo* dominant mutation p.Arg403Cys, very recently reported (Ladds et al., 2018), are often found in other mitochondrial diseases and cannot be considered specific for DRP1 impairment.

In addition to mitochondrial fission, DRP1 is also implicated in the division of peroxisomes (Schrader et al., 2016); to this purpose we investigated peroxisomal morphology and in fibroblasts from Pt. 4 and Pt. 5 we observed organelles significantly longer, larger, and less uniformly distributed into cytoplasm, in contrast with the highly diffused punctuated staining present in control cells; the same condition has been described for other patients with mutations in *DNM1L* (Waterham et al., 2007; Nasca et al., 2016; Zaha et al., 2016) and in transgenic *Drosophila* model expressing a mutant form of *DNM1L* (Chao et al., 2016).

It is not clear why defects of mitochondrial and peroxisomal fission affect predominantly the nervous system. It was demonstrated that DRP1 is required for embryonic and brain development in mice (Ishihara et al., 2009; Wakabayashi et al., 2009). Particularly, DRP1 knockout (KO) caused alteration of mitochondrial morphology and proliferation of embryonic Purkinje cells, suggesting that their development depends highly on mitochondrial division (Wakabayashi et al., 2009). Subsequently, it has been demonstrated that loss of DRP1 led to accumulation of oxidative damage, decreased respiratory function, and neurodegeneration also in post-mitotic Purkinje cells, while DRP1 KO Mouse Embryonic Fibroblasts (MEFs) maintain normal respiration and ATP levels (Kageyama et al., 2012). Given that post-mitotic neurons contain high ROS levels and do not proliferate, the mitochondrial quality control mechanism is essential, while in MEFs, which actively proliferate, mitochondria are produced continuously during cell proliferation and therefore the effect of any oxidative damage may be diluted by the newly formed mitochondria. Moreover, a previous study has shown that the delivery of mitochondria into dendritic protrusions in response to synaptic stimulation is strictly dependent on an efficient mitochondrial transport, that requires DRP1-dependent division (Li et al., 2004); altered mitochondrial distribution likely affects the function and formation of synapses as well as the survival of neurons (Sheng & Cai, 2012; Sheng, 2017). Therefore, the retained DRP1 activity is likely sufficient for organs with limited

mitochondrial remodeling, while impaired DRP1 activity could strongly affect the nervous system, thus explaining the involvement of DRP1 in many neurodegenerative disorders.

Acknowledgments

EBe and RC are supported by the Italian Ministry of Health Ricerca Corrente. DG and CL are supported by Telethon Foundation (Grant GGP15041), the Pierfranco and Luisa Mariani Foundation, the E-Rare project GENOMIT. EBa and PG are supported by MIUR grant FIR2013 (RBFR13IWDS).

The "Cell lines and DNA Bank of Genetic Movement Disorders and Mitochondrial Diseases" of the Telethon Network of Genetic Biobanks (grant GTB12001J) and the EuroBioBank Network supplied biological specimens.

Disclosure statement: The authors declare no conflict of interest.

Public database used

All novel variants reported have been submitted to LOVD database (URl: https://orcid.org/0000-0002-3327-4054).

REFERENCES

Alexiou A, Nizami B, Khan FI, Soursou G, Vairaktarakis C, Chatzichronis S, Tsiamis V, Manztavinos V, Yarla NS, Ashraf GM. 2018. Mitochondrial Dynamics and Proteins Related to Neurodegenerative Diseases. Curr Protein Pept Sci. 19:850-857.

Amati-Bonneau P, Valentino ML, Reynier P, Gallardo ME, Bornstein B, Boissière A, Campos Y, Rivera H, de la Aleja JG, Carroccia R, Iommarini L, Labauge P, et al. 2008. OPA1 mutations induce mitochondrial DNA instability and optic atrophy 'plus' phenotypes. Brain. 131:338-351.

Ardissone A, Tonduti D, Legati A, Lamantea E, Barone R, Dorboz I, Boespflug-Tanguy O, Nebbia G, Maggioni M, Garavaglia B, Moroni I, Farina L, et al. 2018. KARS-related diseases: progressive leukoencephalopathy with brainstem and spinal cord calcifications as new phenotype and a review of literature. Orphanet J Rare Dis 13:45.

Bartsakoulia M, Pyle A, Troncoso-Chandía D, Vial-Brizzi J, Paz-Fiblas MV, Duff J, Griffin H, Boczonadi V, Lochmüller H, Kleinle S, Chinnery PF, Grünert S, et al. 2018. A novel mechanism causing imbalance of mitochondrial fusion and fission in human myopathies. Hum Mol Genet 27:1186-1195.

Baruffini E, Ferrero I, and Foury F. 2010. In vivo analysis of mtDNA replication defects in yeast. Methods 51:426-436. Manual, Cold Spring Harbor Laboratory Press, Cold Spring Harbor, NY.

Bernhardt D, M¨uller M, Reichert AS, Osiewacz HD. 2015. Simultaneous impairment of mitochondrial fission and fusion reduces mitophagy and shortens replicative lifespan. Sci Rep 5:7885.

Bugiani M, Invernizzi F, Alberio S, Briem E, Lamantea E, Carrara F, Moroni I, Farina L, Spada M, Donati MA, Uziel G, Zeviani M. 2004. Clinical and molecular findings in children with complex I deficiency. Biochim Biophys Acta 1659:136-1347.

Cagliani R, Fruguglietti ME, Berardinelli A, D'Angelo MG, Prelle A, Riva S, Napoli L, Gorni K, Orcesi S, Lamperti C, Pichiecchio A, Signaroldi E, et al. 2011. New molecular findings in congenital myopathies due to selenoprotein N gene mutations. J Neurol Sci. 300:107-113.

Cahill TJ, Leo V, Kelly M, Stockenhuber A, Kennedy NW, Bao L, Cereghetti GM, Harper AR, Czibik G, Liao C, Bellahcene M, Steeples V, et al. 2016. Resistance of dynamin-related protein 1 oligomers to disassembly impairs mitophagy, resulting in myocardial inflammation and heart failure. J Biol Chem 291:25762.

Chang CR, Manlandro CM, Arnoult D, Stadler J, Posey AE, Hill RB, Blackstone C. 2010. A lethal de novo mutation in the middle domain of the dynamin-related GTPase Drp1 impairs higher order assembly and mitochondrial division. J Biol Chem 285:32494-32503.

Chao YH, Robak LA, Xia F, Koenig MK, Adesina A, Bacino CA, Scaglia F, Bellen HJ, Wangler MF. 2016. Missense variants in the middle domain of DNM1L in cases of infantile encephalopathy alter peroxisomes and mitochondria when assayed in Drosophila. Hum Mol Genet 25:1846-1856.

Fahrner JA, Liu R, Perry MS, Klein J, Chan DC. 2016. A novel de novo dominant negative mutation in DNM1L impairs mitochondrial fission and presents as childhood epileptic encephalopathy. Am J Med Genet A 170:2002-2011.

Fattori F, Fiorillo C, Rodolico C, Tasca G, Verardo M, Bellacchio E, Pizzi S, Ciolfi A, Fagiolari G, Lupica A, Broda P, Pedemonte M, et al. 2018. Expanding the histopathological spectrum of CFL2-related myopathies. Clin Genet 93:1234-1239.

Francy CA, Alvarez FJ, Zhou L, Ramachandran R, Mears JA. 2015. The mechanoenzymatic core of dynamin-related protein 1 comprises the minimal machinery required for membrane constriction. J Biol Chem 290:11692-11703.

Frank S, Gaume B, Bergmann-Leitner ES, LeitnerWW, Robert EG, Catez F, Smith CL, Youle RJ. 2001. The role of dynamin-related protein 1, amediator ofmitochondrial fission, in apoptosis. Dev Cell 1:515–525.

Gerber S, Charif M, Chevrollier A, Chaumette T, Angebault C, Kane MS, Paris A, Alban J, Quiles M, Delettre C, Bonneau D, Procaccio V, et al. 2017. Mutations in DNM1L, as in OPA1, result in dominant optic atrophy despite opposite effectson mitochondrial fusion and fission. Brain. 140:2586-2596.

Gietz RD, Woods RA. 2002. Transformation of yeast by the LiAc/SS carrier DNA/Peg method. Methods in Enzymology 350: 87-96.

Goffrini P, Ercolino T, Panizza E, Giachè V, Cavone L, Chiarugi A, Dima V, Ferrero I. Mannelli M. 2009. Functional study in a yeast model of a novel succinate dehydrogenase subunit B gene germline missense mutation (C191Y) diagnosed in a patient affected by a glomus tumor. Hum. Mol. Genet 18:1860-1868.

Invernizzi F, D'Amato I, Jensen PB, Ravaglia S, Zeviani M, Tiranti V. 2012. Microscale oxygraphy reveals OXPHOS impairment in MRC mutant cells. Mitochondrion 12:328–335.

Ishihara N, Nomura M, Jofuku A, Kato H, Suzuki SO, Masuda K, Otera H, Nakanishi Y, Nonaka I, Goto Y, Taguchi N, Morinaga H, et al. 2009. Mitochondrial fission factor Drp1 is essential for embryonic development and synapse formation in mice. Nat Cell Biol 11:958-966.

Kageyama Y, Zhang Z, Roda R, Fukaya M, Wakabayashi J, Wakabayashi N, Kensler TW, Reddy PH, Iijima M, Sesaki H. 2012. Mitochondrial division ensures the survival of postmitotic neurons by suppressing oxidative damage. J Cell Biol 197:535-551.

Kaiser C, Michaelis S, Mitchell A. 1994. Methods in Yeast Genetics: a Laboratory Course.

Kim DI, Lee KH, Oh JY, Kim JS, Han HJ. 2017. Relationship Between β-Amyloid and Mitochondrial Dynamics. Cell Mol Neurobiol 37:955-968.

Koch J, Feichtinger RG, Freisinger P, Pies M, Schr¨odl F, Iuso A, Sperl W, Mayr JA, ProkischH,Haack TB. 2016. Disturbed mitochondrial and peroxisomal dynamics due to loss of MFF causes Leigh-like encephalopathy, optic atrophy and peripheral neuropathy. J Med Genet 53:270-278.

Ladds E, Whitney A, Dombi E, Hofer M, Anand G, Harrison V, Fratter C, Carver J, Barbosa IA, Simpson M, Jayawant S, Poulton J. 2018. De novo DNM1L mutation associated with mitochondrial epilepsy syndrome with fever sensitivity. Neurol Genet. 2: e258.

Lenaers G, Hamel C, Delettre C, Amati-Bonneau P, Procaccio V, Bonneau D, Reynier P, Milea D. 2012. Dominant optic atrophy. Orphanet J Rare Dis 7:46.

Li Z, Okamoto K, Hayashi Y, Sheng M. 2004. The importance of dendritic mitochondria in the morphogenesis and plasticity of spines and synapses. Cell 119:873-887.

Losón OC, Song Z, Chen H, Chan DC. 2013. Fis1, Mff, MiD49, and MiD51 mediate Drp1 recruitment in mitochondrial fission. Mol Biol Cell 24:659-667.

Macdonald PJ, Stepanyants N, Mehrotra N, Mears JA, Qi X, Sesaki H, Ramachandran R. 2014. A dimeric equilibrium intermediate nucleates Drp1 reassembly on mitochondrial membranes for fission. Mol Biol Cell. 25:1905-1915.

Monnier N, Romero NB, Lerale J, Nivoche Y, Qi D, MacLennan DH, Fardeau M, Lunardi J. 2000. An autosomal dominant congenital myopathy with cores and rods is associated with a neomutation in the RYR1 gene encoding the skeletal muscle ryanodine receptor. Hum Mol Genet. 9: 2599–2608.

Nasca A, Legati A, Baruffini E, Nolli C, Moroni I, Ardissone A, Goffrini P, Ghezzi D. 2016. Biallelic Mutations in DNM1L are Associated with a Slowly Progressive Infantile Encephalopathy. Hum Mutat 37:898-903.

Nasca A, Rizza T, Doimo M, Legati A, Ciolfi A, Diodato D, Calderan C, Carrara G, Lamantea E, Aiello C, Di Nottia M, Niceta M, et al. 2017. Not only dominant, not only optic atrophy: expanding the clinical spectrum associated with OPA1 mutations. Orphanet J Rare Dis 12:89.

Nasca A, Scotton C, Zaharieva I, Neri M, Selvatici R, Magnusson OT, Gal A, Weaver D, Rossi R, Armaroli A, Pane M, Phadke R, et al. 2017. Recessive mutations in MSTO1 cause mitochondrial dynamics impairment, leading to myopathy and ataxia. Hum Mutat 38:970-977.

Nolli C, Goffrini P, Lazzaretti M, Zanna C, Vitale R, Lodi T, Baruffini E. 2015. Validation of a MGM1/OPA1 chimeric gene for functional analysis in yeast of mutations associated with dominant optic atrophy. Mitochondrion 25:38-48.

Otsuga D, Keegan BR, Brisch E, Thatcher JW, Hermann GJ, Bleazard W, Shaw JM. 1998. The dynamin-related GTPase, Dnm1p, controls mitochondrial morphology in yeast. J Cell Biol 143:333-349.

Pitts KR, McNiven MA, Yoon Y. 2004. Mitochondria-specific function of the dynamin family protein DLP1 is mediated by its C-terminal domains. J Biol Chem 279:50286-94.

Pozo Devoto VM, Falzone TL. 2017. Mitochondrial dynamics in Parkinson's disease: role for α-synuclein? Dis Model Mech 10:1075-1087.

Rapaport D, Brunner M, Neupert W, Westermann B. 1998. Fzo1p is a mitochondrial outer membrane protein essential for the biogenesis of functional mitochondria in Saccharomyces cerevisiae. J Biol Chem 273:20150–20155.

Rizza T, Vazquez-Memije ME, Meschini MC, Bianchi M, Tozzi G, Nesti C, Piemonte F, Bertini E, Santorelli FM, Carrozzo R. 2009. Assaying ATP synthesis in cultured cells: a valuable tool for the diagnosis of patients with mitochondrial disorders. Biochem Biophys Res Commun 383: 58-62.

Ryan CS, Fine AL, Cohen AL, Schiltz BM, Renaud DL, Wirrell EC, Patterson MC, Boczek NJ, Liu R, Babovic-Vuksanovic D, Chan DC, Payne ET. 2018. De Novo DNM1L Variant in a Teenager With Progressive Paroxysmal Dystonia and Lethal Super-refractory Myoclonic Status Epilepticus. J Child Neurol. 33: 651-658.

Santel A, Fuller MT. Control of mitochondrial morphology by a human mitofusin. 2001. J Cell Sci 114:867-874.

Schrader M, Costello JL, Godinho LF, Azadi AS, Islinger M. 2016. Proliferation and fission of peroxisomes - An update. Biochim Biophys Acta 1863:971-983.

Sesaki H, Southard SM, Yaffe MP, Jensen RE. 2003. Mgm1p, a dynamin-related GTPase, is essential for fusionof themitochondrial outermembrane. MolBiolCell 14:2342–2356.

Shamseldin HE, Alshammari M, Al-Sheddi T, SalihMA, AlkhalidiH,Kentab A, RepettoGM,Hashem M, Alkuraya FS. 2012. Genomic analysis of mitochondrial diseases in a consanguineous population reveals novel candidate disease genes. J Med Genet 49:234–241.

Sheffer R, Douiev L, Edvardson S, Shaag A, Tamimi K, Soiferman D, Meiner V, Saada A. 2016. Postnatal microcephaly and pain insensitivity due to a de novo heterozygous DNM1L mutation causing impaired mitochondrial fission and function. Am J Med Genet A 170:1603-1607.

Sheng ZH, Cai Q. 2012. Mitochondrial transport in neurons: impact on synaptic homeostasis and neurodegeneration. Nat Rev Neurosci 13:77-93.

Sheng ZH. 2017. The Interplay of Axonal Energy Homeostasis and Mitochondrial Trafficking and Anchoring. Trends Cell Biol 27:403-416.

Stuppia G, Rizzo F, Riboldi G, Del Bo R, Nizzardo M, Simone C, Comi GP, Bresolin N, Corti S. MFN2-related neuropathies: Clinical features, molecular pathogenesis and therapeutic perspectives. 2015. J Neurol Sci 356:7-18.

ten Brink HJ, Schor DS, Kok RM, Poll-The BT, Wanders RJ, Jakobs C. 1992. Phytanic acid alpha-oxidation: accumulation of 2-hydroxyphytanic acid and absence of 2-

oxophytanic acid in plasma from patients with peroxisomal disorders. J Lipid Res 33:1449-1457.

Vanstone JR, Smith AM, McBride S, Naas T, Holcik M, Antoun G, Harper ME, Michaud J, Sell E, Chakraborty P, Tetreault M, Care4Rare Consortium, et al. 2016. DNM1L-related mitochondrial fission defect presenting as refractory epilepsy. Eur J Hum Genet 24:1084-1088.

Wakabayashi J, Zhang Z, Wakabayashi N, Tamura Y, Fukaya M, Kensler TW, Iijima M, Sesaki H. 2009. The dynamin-related GTPase Drp1 is required for embryonic and brain development in mice. J Cell Biol 186:805-816.

Wangler MF, Assia Batzir N, Robak LA, Koenig MK, Bacino CA, Scaglia F, Bellen HJ. 2018. The expanding neurological phenotype of DNM1L-related disorders. Brain 141:e28.

Waterham HR, Koster J, van Roermund CW, Mooyer PA, Wanders RJ, Leonard JV. 2007. A lethal defect of mitochondrial and peroxisomal fission. N Engl J Med 356:1736–1741.

Yoon G, Malam Z, Paton T, Marshall CR, Hyatt E, Ivakine Z, Scherer SW, Lee KS, Hawkins C, Cohn RD; Finding of Rare Disease Genes (FORGE) in Canada Consortium Steering Committee, 2016. Lethal disorder of mitochondrial fission caused by mutations in DNM1L. J Pediatr 171:313–316.

Youle RJ, van der Bliek AM. 2012. Mitochondrial fission, fusion, and stress. Science 337:1062-1065.

Yu-Wai-Man P, Griffiths PG, Gorman GS, Lourenco CM, Wright AF, Auer-GrumbachM, Toscano A, Musumeci O, Valentino ML, Caporali L, Lamperti C, Tallaksen CM, et al. 2010 Multi-system neurological disease is common in patients with OPA1 mutations. Brain 133:771-786.

Zaha K, Matsumoto H, Itoh M, Saitsu H, Kato K, Kato M, Ogata S, Murayama K, Kishita Y, Mizuno Y, Kohda M, Nishino I, et al. 2016. DNM1L-related encephalopathy in infancy with Leigh syndrome-likephenotype and suppression-burst. Clin Genet 90:472-474.

Zanna C, Ghelli A, Porcelli AM, Karbowski M, Youle RJ, Schimpf S, Wissinger B, Pinti M, Cossarizza A, Vidoni S, Valentino ML, Rugolo M, et al. 2008. OPA1mutations associated with dominant optic atrophy impair oxidative phosphorylationand mitochondrial fusion. Brain 131:352-367.

Figures

Figure 1 MRI pattern of Pt.1 (A-F) obtained at age 6 years and Pt.2 (G-J) obtained at age 7 years. **A**: T2 weighted axial image; **B**: FLAIR weighted axial image; **C-D**: serial DTI images obtained serially in two different days of the same month. In Pt1 the MRI shows signs of global cerebral and cerebellar atrophy, with moderate enlargement of the ventricles. Two serial brain axial DTI weighted MRIs were performed in the same month with a distance of 20 days; the first MRI showed a cortical DTW restriction hyperintensity in the right precentral gyrus, and abnormal DTI restriction hyperintensities corresponding to the pallidum and thalamus of the right hemisphere (**C**). These abnormalities vanished spontaneously 20 days later when a serial brain MRI was performed (**D**). In Pt.2 the T1 weighted sagittal image (**G**) and axial T2 weighted (**I**) and corresponding axial FLAIR weighted images were consistent with a slight global cerebral atrophy, while a cortical DTW restriction hyperintensity was observed only once in the right precentral gyrus (**G-J**) out of 3 MRI scans performed within 3 months of time.

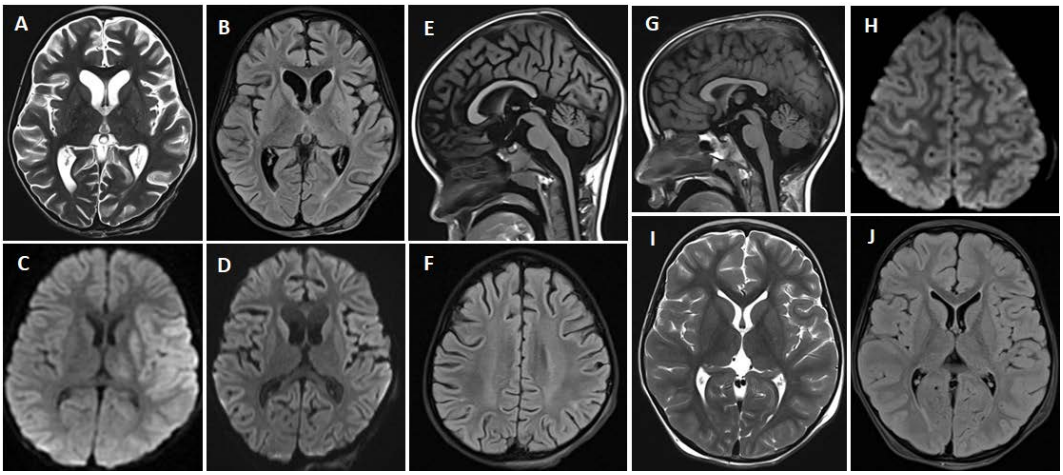

Figure 2 MRI pattern of Pt3. Brain MRI performed at age 7 years. **A**: T2 weighted axial image; **B**: the corresponding FLAIR weighted axial image; **C**: sagittal T1 weighted; **D**: coronal T2 weighted image, showing global severe cortical atrophy that was prominent in both the right hemisphere and the homolateral cerebral peduncle (**A-B**).

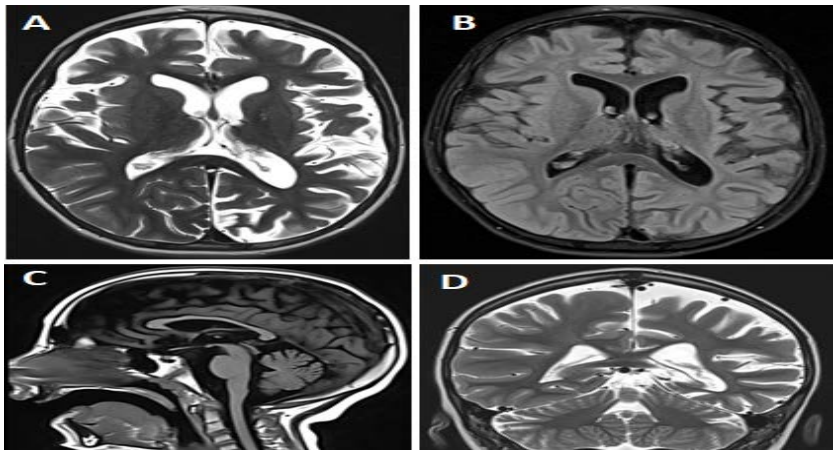

Figure 3 Panel showing the histochemistry of quadriceps muscle samples of Pt.1, Pt.2, Pt.3 and control. The muscle histochemistry of serial sections of three patients with heterozygous dominant mutations in *DNM1L* and stained with cytochrome *c* oxidase (COX) and succinate dehydrogenase (SDH) showed scattered fibers with a patchy reduction of both COX and corresponding SDH staining, with aspects of polymorphic core like areas (left and central panel). Similarly areas of reduced immunoreactivity were observed using the TOMM20 antibody confirming impairment of the mitochondrial network distribution (right panel). These abnormalities were not detected in the muscle biopsy of a patient with biallelic mutations in *OPA1* (last bottom row) already described (Nasca et al., 2017). The plasma membrane is stained in red fluorescence with an antibody against dystrophin.

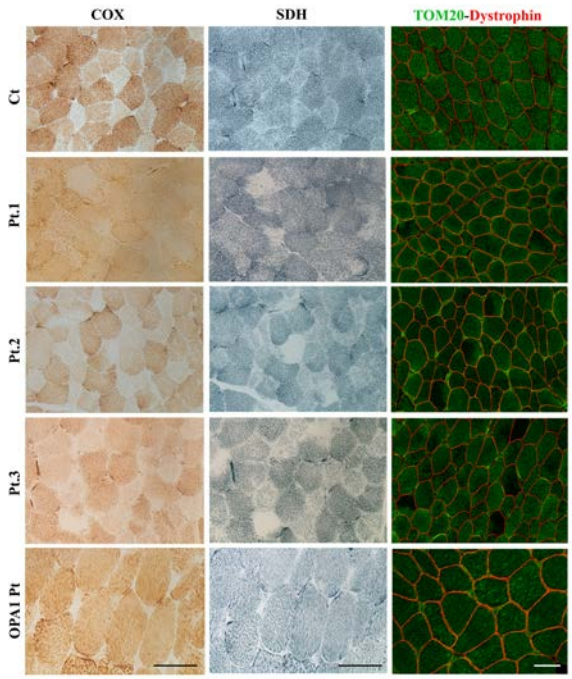

Figure 4 Electropherograms. The variants identified by NGS in *DNM1L* (**A-E**) have been confirmed by Sanger sequencing in all patients and their parents. In **D'** the second variant identified in Pt.4 (c.1535T>C), inherited from the mother.

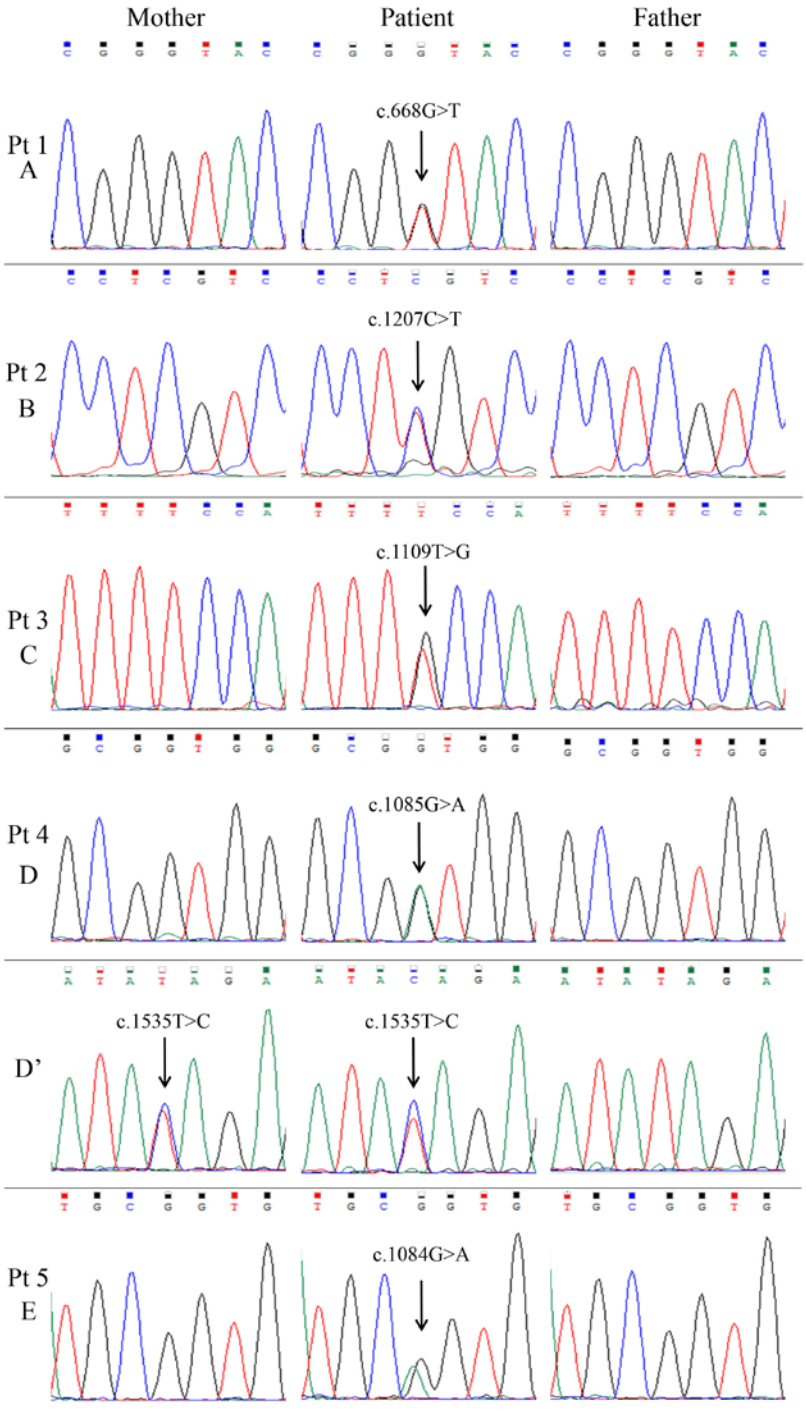

Figure 5 Western blotting analysis. Immunoblot analysis of total lysates from controls (Ct) and patients (Pt) fibroblasts using DRP1, VDAC, and GAPDH antibodies. The latter was used as loading control. The steady state level of DRP1 protein is significantly increased in Pt.3 fibroblasts. Values in the graph are given as the mean ± SD (n = 4 to 5); *, $p<0.05$.

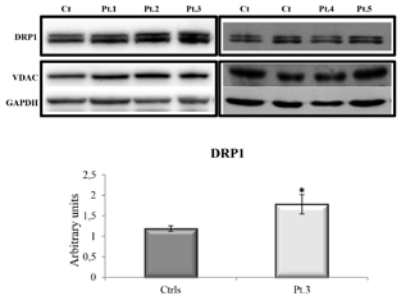

Figure 6 Characterization of the mitochondrial network: analysis by fluorescence microscopy. **A-B:** Representative images of mitochondrial morphology in fibroblasts from Pt.1, Pt.5 and Ct, grown either in glucose or galactose medium. In glucose medium (left panel) patients' fibroblasts are characterized by a mixed population with hyperfused swollen and rod-shaped mitochondria; in galactose medium (right panel) the mitochondrial network of patients' fibroblasts showed a lower tendency to fuse associated with a more disorganized network and an altered mitochondria morphology, with swollen, dots, rings, and "chain-like" structures. (Scale bar: 25 μm).

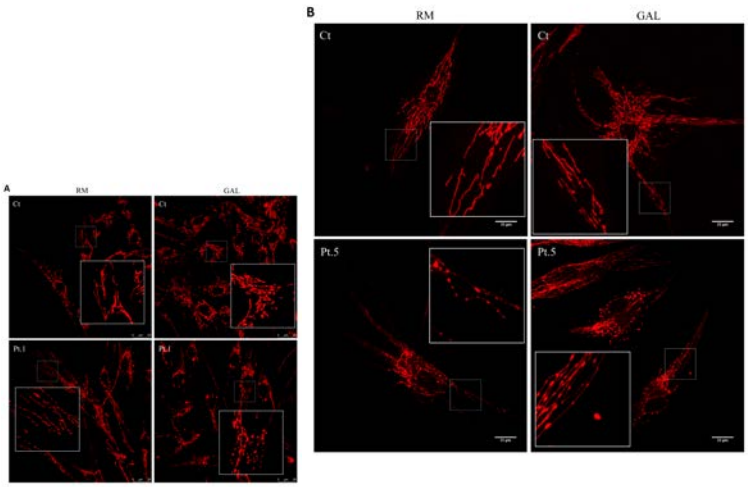

Figure 7 Characterization of the peroxisomal network: analysis by fluorescence microscopy. Immunofluorescence staining with the anti-PMP70 antibody of fibroblasts from Ct, Pt.4 and Pt.5. Patients' fibroblasts displayed organelles longer, larger, and less uniformly distributed into cytoplasm compared to control (Scale bar: 25 μm). A form factor ("circularity") value of 1.0 indicates a perfect circle; values approaching to 0.0 indicate increasingly elongated shapes.

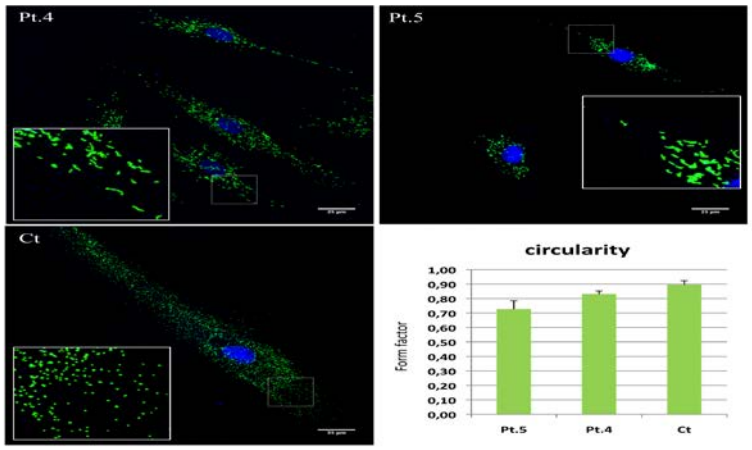

Figure 8 Functional studies in yeast. **A**: Phenotypic analysis of haploid strains through spot assay. Serial cell dilutions ($5x10^4$, $5x10^3$, $5x10^2$ and $5x10^1$ cells/spot) of *dnm1Δ* haploid strain transformed with *DNM1* wild type or mutant alleles were spotted on SC medium supplemented with either 2% glucose or 2% glycerol. Pictures were taken after a 3-days incubation at 37°C. **B**: *Petite* frequency of *dnm1Δ* haploid strain transformed with *DNM1* wild type or mutant alleles. Values are means of six to eight independent clones ± SD. **($p<0.01$) and ***($p<0.001$) in a ANOVA test followed by a Bonferroni's test. **C**: Respiratory activity of *dnm1Δ* haploid strain transformed with *DNM1* wild type or mutant alleles. Values are means ± SD of experiments on five clones and have been normalized to the respiratory activity of the *DNM1* wt strain. *($p<0.05$) and ***($p<0.001$) using ANOVA with post-hoc Bonferroni's test. **D**: Respiratory activity of *DNM1*/*dnm1Δ* diploid strain transformed with *DNM1* wild type or mutant alleles. Values are means ± SD of experiments on five clones and have been normalized to the respiratory activity of the *DNM1* wt strain. *($p<0.05$) and ***($p<0.001$) using ANOVA with post-hoc Bonferroni's test.

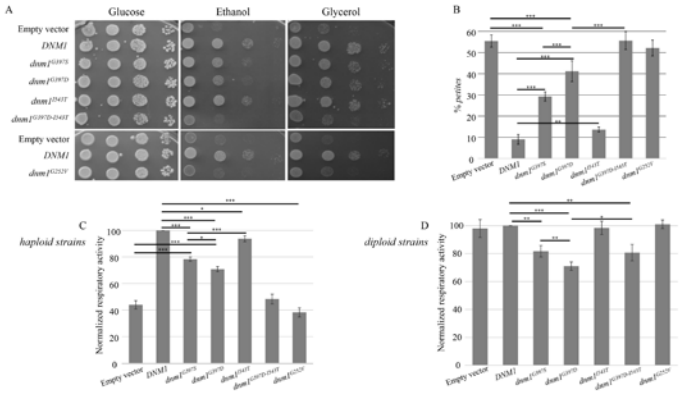

Figure 9 Conservation and structural mapping of residues affected by the missense mutations G223V, G362D, F370C, and R403C. **A**: multiple sequence alignment among species (invariant columns are grayed). **B**: mapping of G223 on the crystal structure of a dimeric human dynamin-1-like protein (PDB 3W6O; residues 215-221, colored in magenta, are important for GTP binding; the cocrystallized nucleotide analogue is shown as sticks). Mapping of G362 (**C**), F370 (**D**), and R403 (**E**) on dynamin tetramer (PDB 5A3F). The red dotted lines indicate the disordered regions in which R403 is hosted in two of the four dynamin monomers. The different dynamin chains are in distinct colors. Amino acid numbering is made according to the isoform 1 of dynamin-1-like protein (NP_036192.2).